remote sensing

MDPI

Article

Unraveling Regional Patterns of Sea Level Acceleration over the China Seas

Ying Qu [1,*], Svetlana Jevrejeva [2] and Shijin Wang [3]

[1] School of Geography Science and Geomatics Engineering, Suzhou University of Science and Technology, Suzhou 215009, China
[2] National Oceanography Center, 6 Brownlow Street, Liverpool L3 5DA, UK; sveta@noc.ac.uk
[3] Yulong Snow Mountain Cryosphere and Sustainable Development Field Scientific Observation and Research Station, Northwest Institute of Eco-Environment and Resources, Chinese Academy of Sciences, Lanzhou 730000, China; wangshijin@lzb.ac.cn
* Correspondence: yingqu@usts.edu.cn; Tel.: +86-18518529943

Abstract: Accelerated sea level rise is placing coastal communities in a vulnerable position; however, the processes underlying sea level acceleration in China remain uncertain. In this study, we examine the sea level acceleration and its contributors over the China Seas. We calculate acceleration along the Chinese coast using satellite altimetry and tide gauge records. During the satellite altimetry era, sea level acceleration from tide gauge records varies across all stations, reaching up to 0.30 ± 0.20 mm/yr^2, while satellite altimetry could underestimate/overestimate the sea level acceleration in most locations. Acceleration near the coast, except in the Bohai Sea, is mainly driven by changes in the mass component. In contrast, for the open ocean, changes in steric sea level are the main contributor to sea level acceleration. The evolution of spatial acceleration patterns over the China Seas reveals that the ENSO and PDO variabilities dominate the changing patterns of sea level acceleration in the open ocean, including the Philippine Sea through steric sea level, and changes in most coastal locations are due to the non-steric component.

Keywords: sea level acceleration; tide gauge; satellite altimetry; steric; mass change

check for updates

Citation: Qu, Y.; Jevrejeva, S.; Wang, S. Unraveling Regional Patterns of Sea Level Acceleration over the China Seas. *Remote Sens.* **2023**, *15*, 4448. https://doi.org/10.3390/rs15184448

Academic Editor: Weimin Huang

Received: 15 July 2023
Revised: 14 August 2023
Accepted: 4 September 2023
Published: 9 September 2023

Copyright: © 2023 by the authors. Licensee MDPI, Basel, Switzerland. This article is an open access article distributed under the terms and conditions of the Creative Commons Attribution (CC BY) license (https://creativecommons.org/licenses/by/4.0/).

1. Introduction

Sea level rise is regarded as one of the important consequences of climate change, with implications for regions worldwide [1]. Detecting sea level acceleration is of vital importance, especially for coastal communities, as many large cities are located along the coastline, so accelerated sea level rise will place them under greater risks in the future. This includes densely populated coastal areas of China, which has 32 thousand kilometers of coastline with ever-increasing infrastructure [2–4].

This consensus has been reached about global sea level rise [1], with proxy and instrumental observations providing the evidence of global sea level acceleration over the last two centuries [5–9], leading to a more severe economic impact in the coastal areas due to an increased frequency of coastal flooding and intensified coastal erosion [10]. In China, coastal areas account for only 13% of land area, but sustain 43% of the national population and over 62% of GDP [11], making them vulnerable to sea level rise under all climate change scenarios [12,13]. Future development and adaptation plans require robust estimates of sea level rise and its acceleration, identifying when and how the local sea level deviates from simulated future sea level projections.

Sea level variations are the sum of changes in the steric component (that is produced by water expansion or contraction) and the mass component, which results from the contribution of mountain glaciers, ice sheets in Greenland and the Antarctic, and land water storage [1]. Ice sheets melting has been proven to be the main contributor to global mean sea level acceleration during the satellite altimetry era, while for the regional pattern [14],

internal variations, including ENSO and PDO, could play the dominant role [14–16]. Various sea level contributors define the complex spatial patterns of regional sea level changes, and there is a lack of understanding about the main physical mechanisms driving sea level acceleration along the coast of China. Thus, understanding the main drivers for sea level acceleration is crucial for projecting future sea levels in China.

In this study, we unravel regional patterns of sea level acceleration for coastal areas in China, examine the contribution of steric and mass-induced sea level components to sea level acceleration, and explore the role of ENSO and PDO in the changes in acceleration patterns.

2. Materials and Methods

2.1. Tide Gauge Records

Monthly tide gauge records are obtained from PSMSL [17,18], among which NPQB come from the merging of North Point and Quarry Bay stations as they have matching datum information [19]. NPQB has the longest record of 71 years while Shanwei and Beihai have the shortest record of 20 years. Detailed information about the tide gauge records is presented in Table 1. Inverse barometer effects are corrected for the tide gauge records to compare with the satellite altimetry data, using monthly sea level pressure data from NCEP/NCAR reanalysis datasets [20]. Sea level acceleration at tide gauge locations measured using satellite altimetry is estimated from the time series within the area of $\pm 0.2^\circ$ lat/lon around the station.

Table 1. Selected tide gauge records and the record length in years used in this study and the sea level acceleration (mm/yr^2) at selected locations after removing the seasonal cycle.

Station Name	Longitude (°E)	Latitude (°N)	Time Span	Completeness (%)	Record Length in Years	Acceleration (mm/yr^2)
Qinhuangdao	119.60	39.90	1950–1994	99	45	0.04 ± 0.06
Tanggu	117.72	39.00	1975–1994	100	20	2.08 ± 0.54
Dalian	121.68	38.87	1970–2021	97	52	0.05 ± 0.04
Yantai	121.38	37.53	1954–1994	100	41	-0.33 ± 0.12
Shijiusu	119.55	35.38	1975–1994	100	20	1.02 ± 0.32
Lianyungan	119.45	34.75	1975–1994	100	20	1.50 ± 0.38
Lusi	121.62	32.13	1969–2020	93	52	-0.05 ± 0.04
Kanmen	121.28	28.08	1959–2021	99	63	0.08 ± 0.03
Xiamen	118.07	24.45	1954–2004	100	51	0.00 ± 0.05
Shanwei	115.35	22.75	1975–1994	100	20	0.55 ± 0.40
Zhapo	111.82	21.58	1959–2021	99	63	0.05 ± 0.03
Beinhai	109.08	21.48	1975–1994	100	20	0.20 ± 0.30
Xi Sha	112.33	16.83	1990–2021	99	32	0.09 ± 0.23
Nan Sha	112.88	9.55	1998–2021	83	24	0.38 ± 0.27
Macau	113.55	22.20	1925–1985	96	61	-0.09 ± 0.04
NPQB	114.21	22.29	1950–2020	99	71	0.11 ± 0.02
Tai Po Kau	114.18	22.44	1963–2020	95	58	0.07 ± 0.04
Tsim Bei Tsui	114.01	22.49	1974–2020	84	47	0.24 ± 0.07
Tai Miu Wan	114.29	22.27	1997–2020	94	24	0.23 ± 0.41
Shek Pik	113.89	22.22	1998–2020	97	23	0.41 ± 0.32
Keelung II	121.73	25.13	1956–1995	100	40	0.43 ± 0.05

2.2. Satellite Altimetry

Gridded monthly sea level anomalies from satellite altimetry are used. The satellite altimetry product comes from NASA JPL (Jet Propulsion Laboratory, Pasadena, CA, USA) (https://podaac.jpl.nasa.gov/dataset/SEA_SURFACE_HEIGHT_ALT_GRIDS_L4_2SATS_5DAY_6THDEG_V_JPL2205, accessed on 1 April 2023), which processes data from several altimeters. The sea level anomalies are available on a resolution of $0.17^\circ \times 0.17^\circ$ (lat/lon) from 1993 to 2020 and are corrected for inverted barometer (IB) effects.

2.3. Steric Component

To determine the contribution to sea level acceleration, we examine the acceleration of both the steric and mass components.

For studying the steric sea level contribution to acceleration, we use the IAP steric sea level obtained from the Institute of Atmospheric Physics, Chinese Academy of Sciences (http://www.ocean.iap.ac.cn/ftp/cheng/IAP_Gridded_Steric_sea_level_upper2000m/, accessed on 10 December 2022) on a horizontal resolution of $1^\circ \times 1^\circ$ for upper 2000 m layers, which has advantages in reducing the sampling errors as it uses available observations to infill data gaps with an improved interpolation method [21,22]. We re-grid the IAP steric sea level to the same resolution as the NASA satellite altimetry to make it comparable.

2.4. Mass Component

Mass-induced sea level can be computed from water mass change in the ocean monitored by the Gravity Recovery and Climate Experiment (GRACE) [23–25]. Gridded monthly liquid water equivalent thickness product on a resolution of $0.5^\circ \times 0.5^\circ$ derived from GRACE/GRACE-FO, starting from 2002 to the present, are obtained from JPL (https://grace.jpl.nasa.gov, accessed on 1 April 2023). We re-grid GRACE data to the resolution of NASA satellite altimetry data ($0.17^\circ \times 0.17^\circ$) as well. GRACE observations are used to determine the contribution of mass redistribution to regional sea level acceleration.

The version of data we use is based on GRACE and GRACE-FO with a Coastline Resolution Improvement (CRI) filter applied to reduce signal leakage errors that span coastlines.

2.5. Climate Indexes

In this study, two dominant climate indexes influencing the regional sea level acceleration are considered, ENSO (El Niño–Southern Oscillation) and PDO (Pacific Decadal Oscillation), as they are the two major climate modes influencing the sea level pattern in the Pacific Ocean [26]. MEI index (https://psl.noaa.gov/enso/mei/data/meiv2.data, accessed on 1 April 2023), which represents the ENSO signal, is adopted; it is the Multivariate ENSO index which combines several climate variables over the tropical Pacific. PDOs (https://www.ncdc.noaa.gov/teleconnections/pdo/, accessed on 1 April 2023) are calculated from sea surface temperature, for north of 20°N in the Pacific Ocean [26–28].

2.6. Methods

We adopt a regression model to estimate the sea level acceleration around the China Seas, and we remove annual and semi-annual cycles from the time series by applying a 6- and 12-month least-square fit before applying the model.

$$h = a + bt + ct^2 \tag{1}$$

where t is time. a, b, c coefficients are estimated using the least-squares fit; a is a constant and b denotes the linear trend while the acceleration rate is twice the coefficient c. h denotes the preprocessed sea level time series. We assume that vertical land motion such as Glacial Isostatic Adjustment is linear and does not affect the sea level acceleration. The calculations of acceleration are based on the function *polyfit* in MATLAB, which estimates the sea level acceleration using a least-square quadratic fit following previous studies [28,29]. The confidence interval at 95% level is estimated with the function *polyparci*, which calculates the covariance matrix based on the key statistics provided by *polyfit*. The standard deviation is measured of what the *polyfit* model is unable to fit in the observations.

To examine the contribution of ENSO and PDO variability to regional sea level acceleration, we remove the annual and semi-annual cycles from the time series at first, and then we use a linear regression model [28,29] to fit the climate indexes [24]:

$$h = a_0 + a_1 t + a_2 t^2 + a_3 MEI(t) + a_4 PDO(t) \tag{2}$$

Here, t is time, coefficients a_0 to a_4 are estimated with the least-squares fit, and h denotes the preprocessed sea level time series. The time series of MEI and PDO indexes are filtered following Zhang and Church [30], as the MEI index is high-pass filtered while the PDO index is low-pass filtered. The part related to ENSO and PDO variabilities in Equation (2) is removed from h to exclude their contribution [16,30].

3. Results

3.1. Estimates of Sea Level Acceleration along the Coast of China

In our study, we denote 'the China Seas' as a wider region, which is located between 100–180°E and 0–50°N; thus, several different countries are included. We select all 21 tide gauge stations with records no less than 20 years and completeness higher than 80% to study the sea level acceleration around the China coast. All selected tide gauge stations in our study area as well as the bathymetry map are shown in Figure 1. Among all these stations, Tai Po Kau, Tsim Bei Tsui, Tai Miu Wan, and Shek Pik are close to each other, and so are presented in the figure but are not labeled due to the limited space.

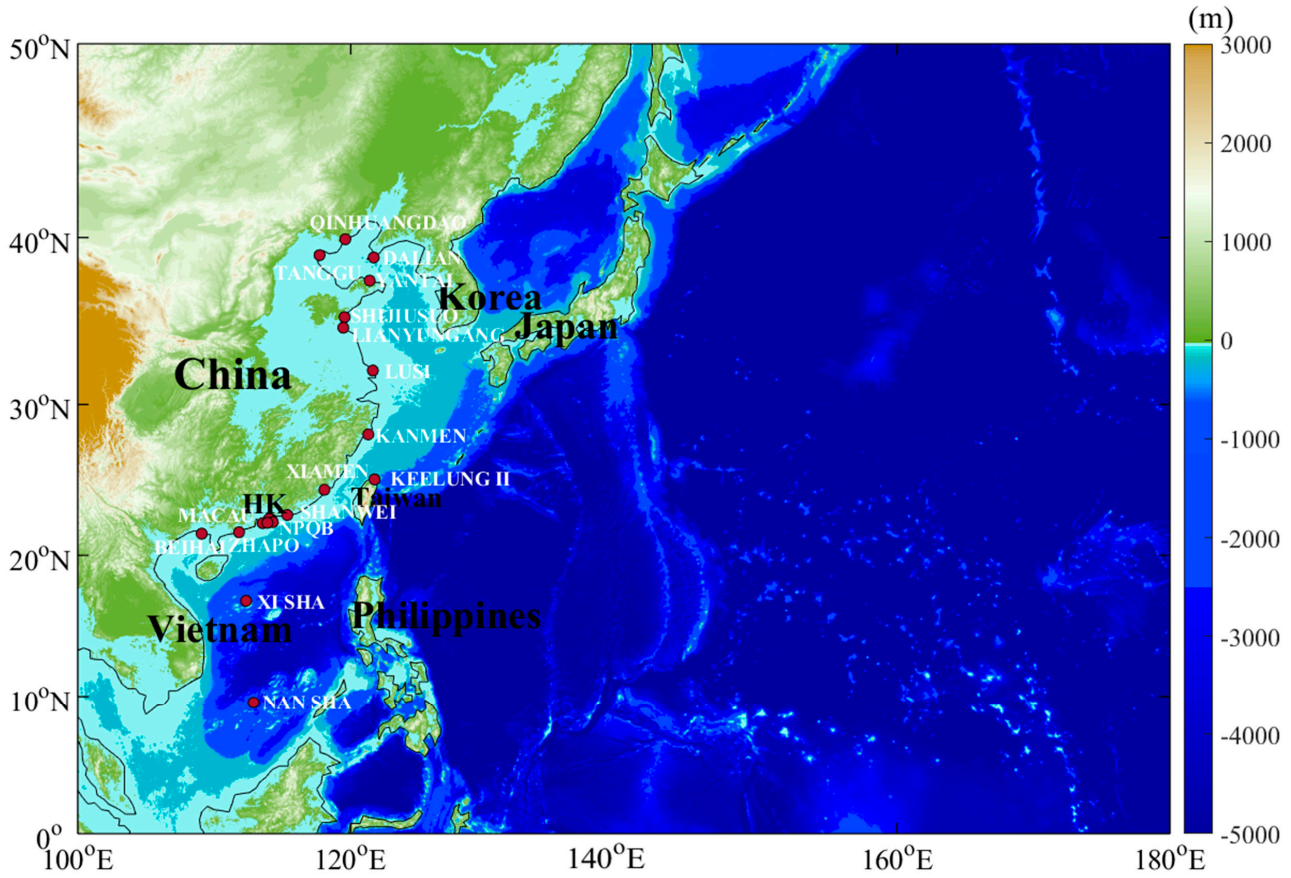

Figure 1. The spatial distribution of 21 tide gauge locations and bathymetry within the study area.

After removing the seasonal cycle, the sea level acceleration at each tide gauge station is estimated using a least-square fit (see Methods) over the observational period (Table 1). Table 1 shows that the estimates of acceleration range from -0.05 ± 0.04 mm/yr^2 in Lusi (1969–2020) to 0.41 ± 0.32 mm/yr^2 in Shek Pik (1998–2020) for records ending after the 2000s, and depend on the length of time series. Acceleration for the longest sea level record (1950–2020) at NPQB is 0.11 ± 0.02 mm/yr^2.

Accelerations for all 21 tide gauge records with increasing lengths from 20 years to the whole period of observations before and after removing the seasonal cycle are shown in Figure 2a,b, respectively, while the difference between them is shown in Figure 2c. We estimate the acceleration from twenty years to the whole period using moving windows

for record lengths longer than twenty years; different colors represent different stations. All tide gauge records show multidecadal variations in estimates of sea level acceleration, suggesting that there are 20–30 year oscillations in sea level records. The scatter of sea-level-acceleration values decreases with an increase in record length. Figure 2c shows that estimates of acceleration in records shorter than 30 years are sensitive to seasonal variability, the removal of seasonality could change the acceleration by -0.30 mm/yr^2 (Tsim Bei Tsui) to 0.22 mm/yr^2 (Nan Sha) for a record length of 20 years.

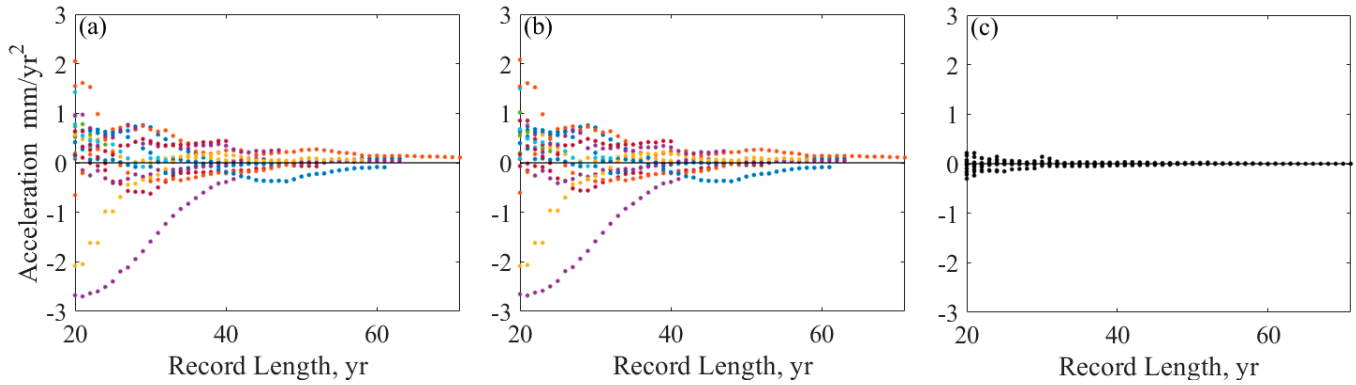

Figure 2. Acceleration (mm/yr^2) vs. record lengths using 21 tide gauge records (represented by different colored dots) before removing the seasonal cycle (**a**). Acceleration (mm/yr^2) vs. record lengths using 21 tide gauge records (represented by different colored dots) after removing the seasonal cycle (**b**) and the difference between before and after removing the seasonal cycle (**c**).

Using satellite altimetry data, we examine the evolution of acceleration in time depending on the lengths of time series for the near coastal locations and open ocean. We apply variable windows from 10 to 300 months to sea level time series near the coastline (within 0.2° to the coast) and averaged over the study area presented in Figure 1 between 1993 and 2020. By sliding the windows month-by-month over the satellite altimetry era, we show the evolution of sea level acceleration depending on the length of window and time span of data. Figure 3 shows that the sea level has been evolving with positive and negative accelerations since 1993. The reversal between positive and negative accelerations is more frequent near the coastline compared with the open-ocean study area.

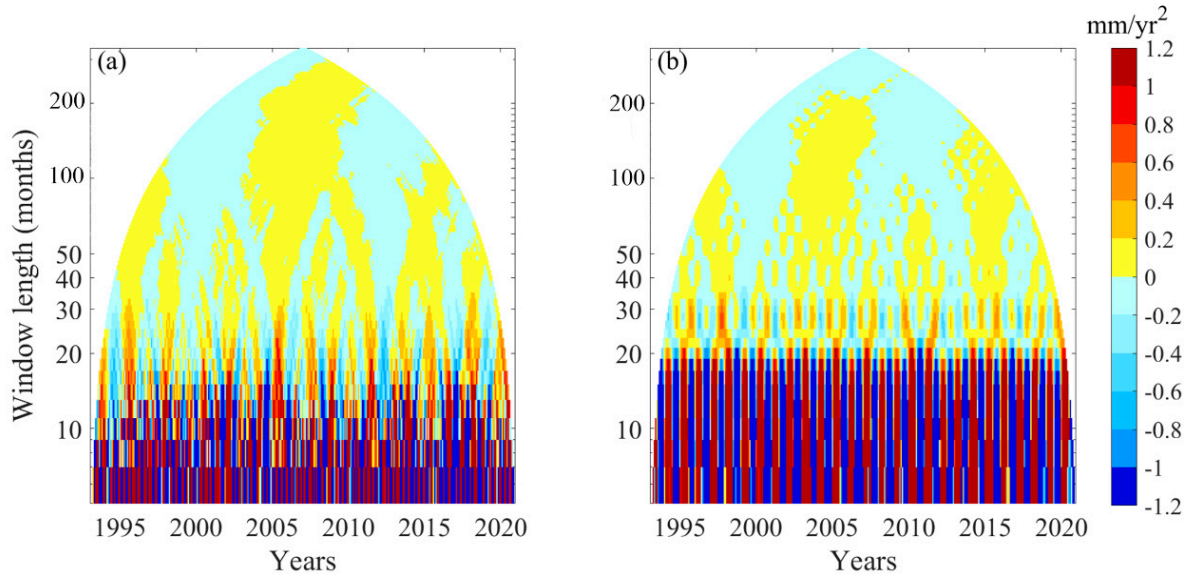

Figure 3. Estimates of sea level acceleration along the coastline (**a**) and for the open-ocean study area (**b**) calculated for satellite altimetry data since 1993.

3.2. Patterns in Regional Sea Level Acceleration

We calculate the sea level acceleration from satellite altimetry, IAP steric, and the differences between them (e.g., acceleration in non-steric component) as shown in Figure 4a–c. There is an agreement between the patterns for sea level acceleration from satellite altimetry and for steric sea level in the open ocean areas, e.g., around the Philippine Sea: they both show negative acceleration. Along the coast, estimates of acceleration from tide gauge records, available for 1993–2020, vary from -0.07 ± 0.19 mm/yr^2 to 0.30 ± 0.20 mm/yr^2, with large error bars (Table 2). Note that only eight tide gauge records are available over the satellite altimetry era (Table 2). Most tide gauge locations show positive acceleration, except Dalian and Lusi, while for all locations, the acceleration in steric sea level is negative. There is almost no contribution to sea level acceleration from the steric component in coastal locations (Figure 4a–c, Table 2) except Dalian, suggesting that a possible mass redistribution accounts for the acceleration (Figure 4a–c, Table 2). The acceleration for longer tide gauge records since 1970 could not be explained by the steric component in most locations.

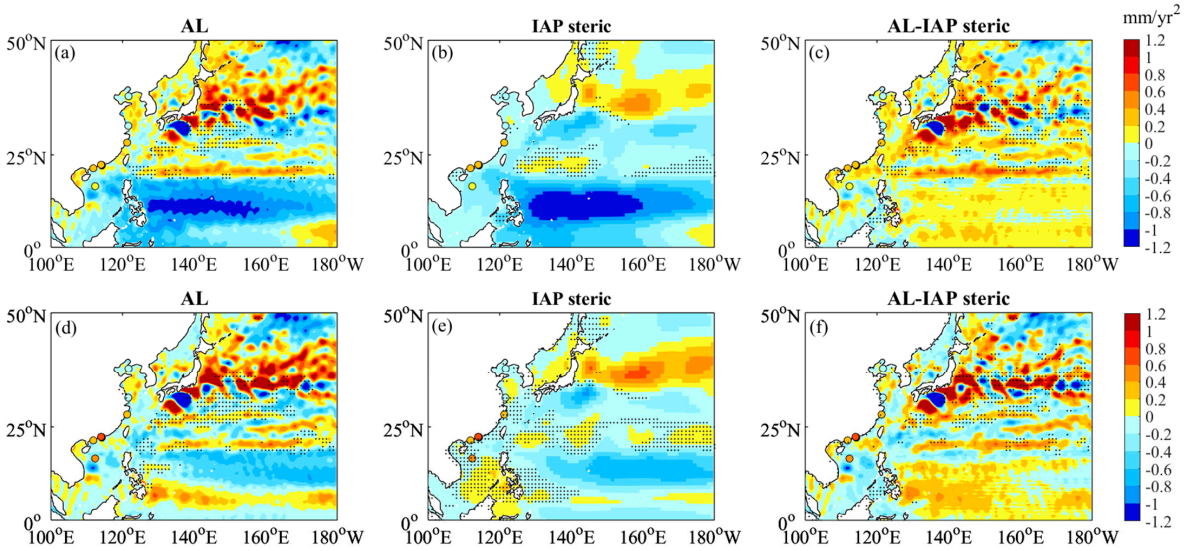

Figure 4. Sea level acceleration (Units: mm/yr^2) from satellite altimetry, IAP steric, and the differences between satellite altimetry and IAP steric during 1993–2020 before (**a**–**c**) and after (**d**–**f**), removing the ENSO and PDO variabilities. Colored circles represent the sea level acceleration of tide gauge records during 1993–2020. Stippling indicates regions with no significant difference at the 95% level.

Table 2. Sea level acceleration (mm/yr^2) from tide gauge records, steric sea level, and satellite altimetry over different periods.

Tide Gauge	Time of Span	1970–2020		1993–2020		
		TG [a]	ST [b]	TG	AL [c]	ST
Dalian	1970–2021	0.04 ± 0.04	0.04 ± 0.01	-0.05 ± 0.15	0.03 ± 0.03	-0.04 ± 0.03
Lusi	1969–2020	-0.07 ± 0.04	N/A [d]	-0.07 ± 0.19	-0.23 ± 0.01	-0.00 ± 0.01
Kanmen	1959–2021	0.15 ± 0.04	N/A [d]	0.30 ± 0.20	-0.41 ± 0.01	-0.03 ± 0.01
Zhapo	1959–2021	0.11 ± 0.04	N/A [d]	0.22 ± 0.20	-0.11 ± 0.20	-0.08 ± 0.03
Xi Sha	1990–2021	0.02 ± 0.24 [※]	0.01 ± 0.03 [※]	0.14 ± 0.31	-0.38 ± 0.12	-0.30 ± 0.12
NPQB	1950–2020	0.05 ± 0.05	N/A [d]	0.02 ± 0.20	0.17 ± 0.02	-0.06 ± 0.02
Tai Po Kau	1963–2020	0.17 ± 0.05	N/A [d]	0.26 ± 0.20	0.18 ± 0.02	-0.06 ± 0.02
Tsim Bei Tsui	1974–2020	0.22 ± 0.07 [※]	N/A [d,※]	0.29 ± 0.23	0.18 ± 0.02	-0.06 ± 0.02

[※] Denotes tide gauge records starting later than 1970; we calculate from the record over the maximum time span between 1970 and 2020. [a] Tide Gauge. [b] Steric. [c] Altimetry. [d] N/A denotes that the steric sea level acceleration is negligible compared to tide gauges and altimetry.

The acceleration (Table 2) near the tide gauge locations from satellite altimetry is underestimated compared with tide gauge records in most locations, although there are larger error bars in the estimates of acceleration from tide gauge records than those in satellite altimetry.

Strong negative acceleration in the Philippine Sea and the open ocean (Figure 4a) is statistically significant and in agreement with steric sea level acceleration (Figure 4b). The magnitude of acceleration from satellite altimetry and IAP steric sea level in the Philippine Sea and open ocean areas is reduced with the removal of the ENSO and PDO variability (Figure 4d–f).

Evolutions of sea-level-acceleration patterns in time, using a 20-year moving window, are shown in Figures 5 and 6 (for satellite altimetry) and Figures 7 and 8 (for steric). Figures 5–8 demonstrate that acceleration patterns are varying along the coast and in open ocean areas. After removing the ENSO and PDO variabilities, sea level acceleration from satellite altimetry (Figure 6) for each 20-year window shows an increase in acceleration in the Philippine Sea and around open ocean areas compared with Figure 5. Such time-variable changing patterns are also revealed in IAP steric (Figure 8), suggesting that steric changes mainly contribute to the evolution of the sea-level-acceleration patterns in the Philippine Sea and its open ocean areas.

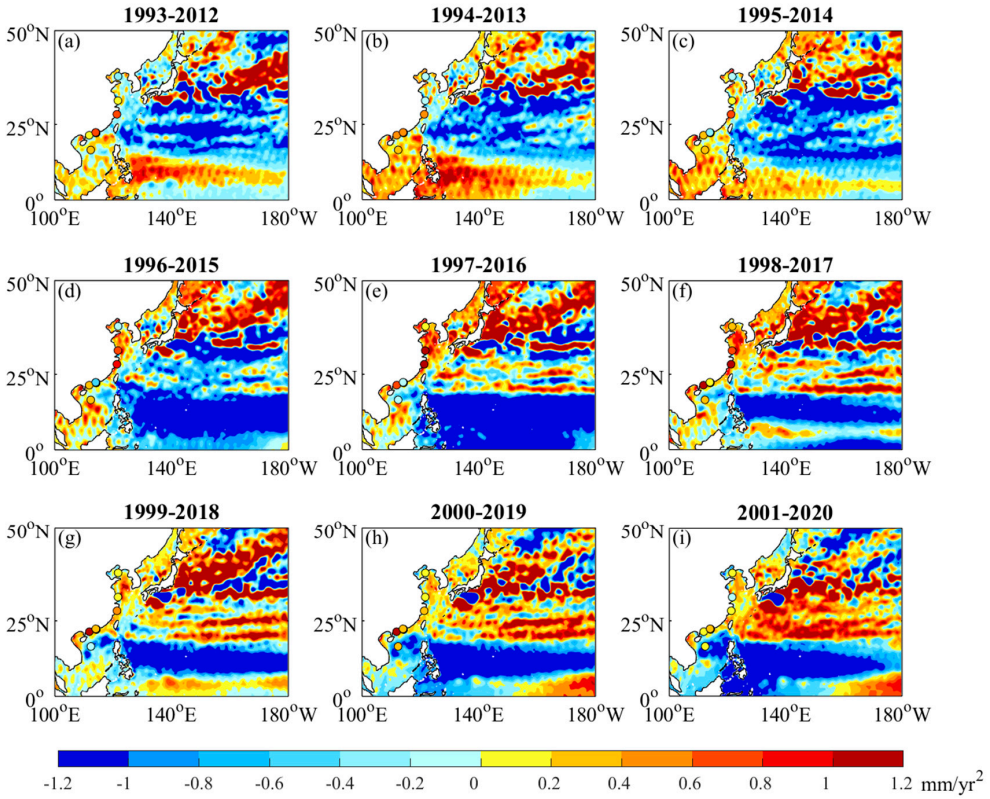

Figure 5. Sea level acceleration for a 20-year moving window from satellite altimetry and selected tide gauge locations; Colored circles represent the sea level acceleration of tide gauge records during the selected period.

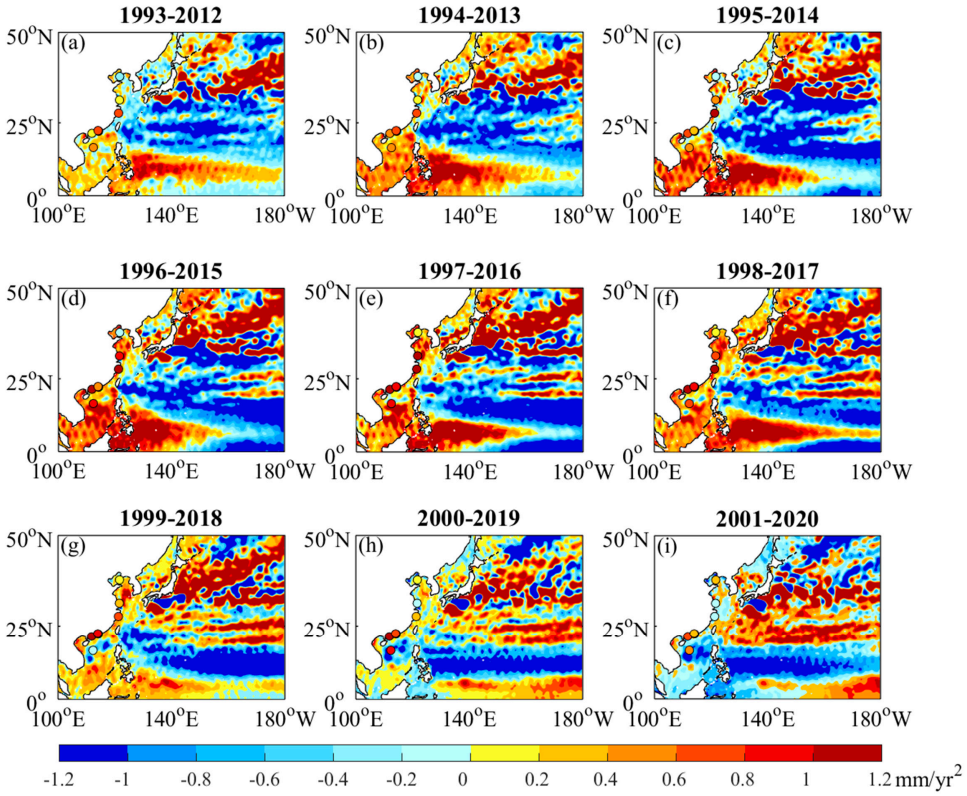

Figure 6. Sea level acceleration for a 20-year moving window from satellite altimetry and selected tide gauge locations after removing ENSO and PDO variabilities; colored circles represent the sea level acceleration of tide gauge records after removing ENSO and PDO variabilities during the selected period.

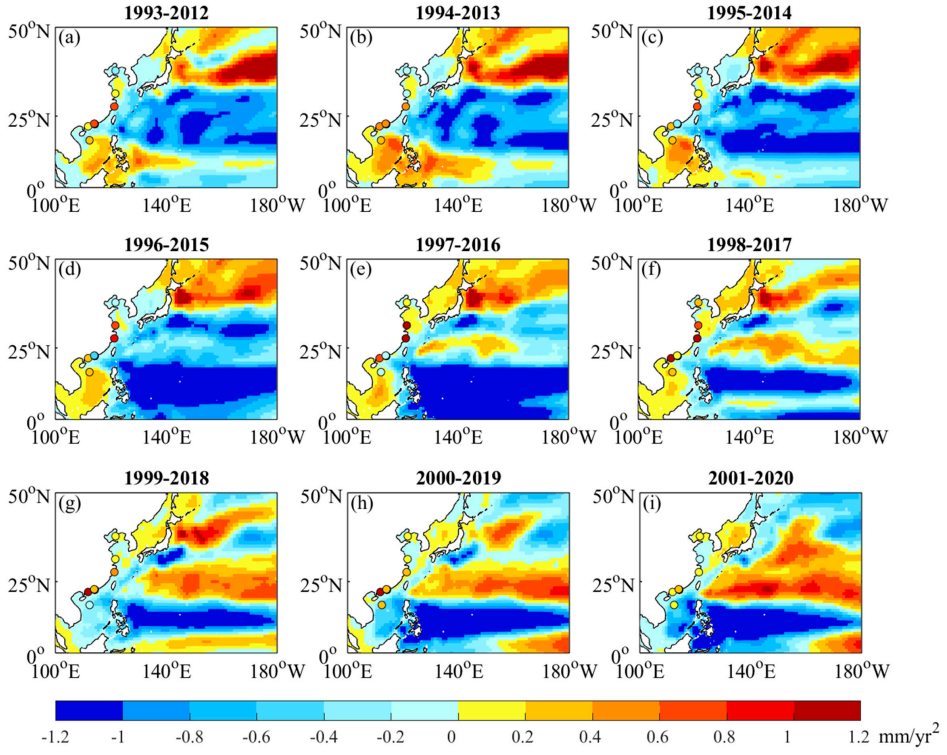

Figure 7. Sea level acceleration for a 20-year moving window from IAP steric and selected tide gauge locations; colored circles represent the sea level acceleration of tide gauge records during the selected period.

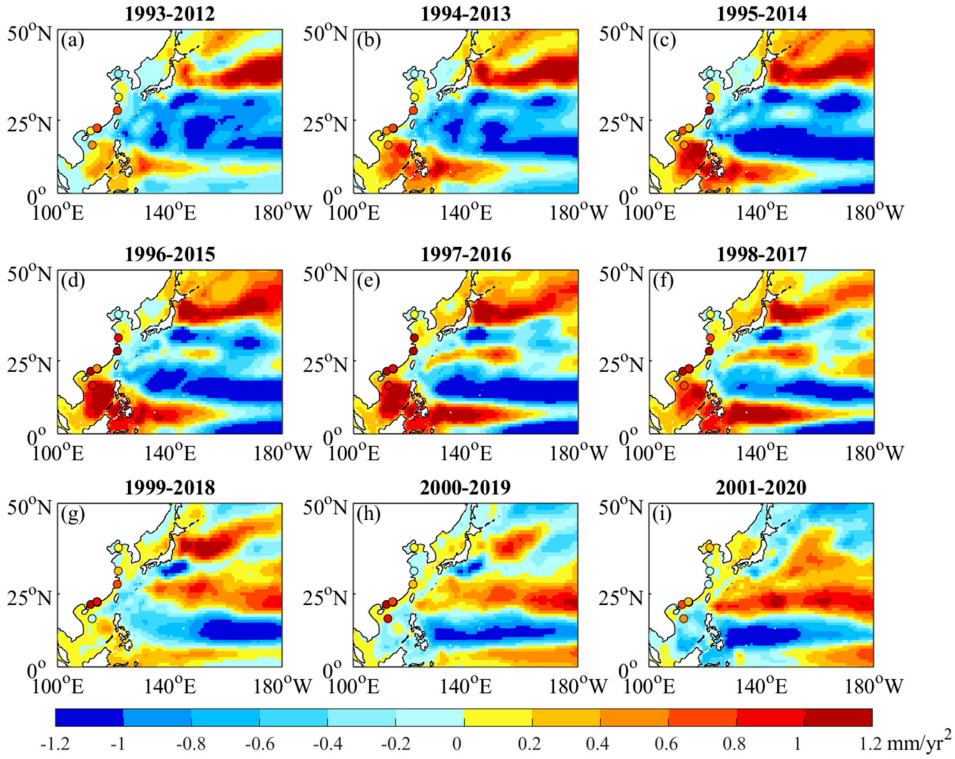

Figure 8. Sea level acceleration for a 20-year moving window from IAP steric and selected tide gauge locations after removing ENSO and PDO variabilities; colored circles represent the sea level acceleration of tide gauge records after removing ENSO and PDO variabilities during the selected period.

We calculate the sea level accelerations from tide gauge records (Table 3) and IAP steric (Table 4) before and after removing the ENSO and PDO variabilities at individual locations for a 20-year moving window. While along the coast tide, gauge records generally show a coherent pattern after the removal of ENSO and PDO variabilities, which could contribute up to 0.32 mm/yr^2 of coastal sea level acceleration at certain tide gauge locations (Tables 3 and 5), the steric component is not considered as the main contributor (Table 4). ENSO and PDO variabilities are proven to have more pronounced impacts for some coastal regions than the global region.

Table 3. Sea level acceleration (mm/yr^2) from tide gauge records before and after removing ENSO and PDO variabilities for a 20-year moving window.

	1993–2012		**1994–2013**		**1995–2014**		**1996–2015**		**1997–2016**	
Tide Gauge	**Before**	**After**	**Before**	**After**	**Before**	**After**	**Before**	**After**	**Before**	**After**
Dalian	−0.27	−0.28	−0.13	−0.06	−0.15	−0.11	−0.05	−0.10	0.19	0.04
Lusi	0.10	0.08	−0.08	0.16	0.19	0.51	0.61	0.86	1.19	1.24
Kanmen	0.62	0.62	0.47	0.68	0.77	1.01	0.93	1.20	1.26	1.44
Zhapo	0.03	0.06	0.44	0.59	0.37	0.75	0.35	1.03	0.75	1.42
Xi Sha	0.38	0.43	0.35	0.44	0.31	0.56	0.23	0.92	−0.01	0.92
NPQB	−0.30	−0.25	0.44	0.61	0.80	1.10	0.93	1.52	1.14	1.78
Tai Po Kau	0.62	0.63	1.29	1.23	1.35	1.46	0.89	1.35	0.89	1.42
Tsim Bei Tsui	0.63	0.66	0.47	0.71	−0.28	0.38	−0.53	0.47	−0.02	0.87
	1998–2017		1999–2018		2000–2019		2001–2020			
Tide Gauge	Before	After	Before	After	Before	After	Before	After		
Dallian	0.22	0.17	0.00	0.06	0.20	0.11	0.46	0.34		
Lusi	0.61	0.74	0.18	0.27	0.03	−0.12	−0.06	−0.17		
Kanmen	1.11	1.31	0.59	0.71	0.34	0.28	0.11	−0.01		
Zhapo	1.04	1.50	1.16	1.45	1.02	1.22	0.70	0.79		
Xi Sha	0.26	0.73	−0.17	−0.03	0.33	0.81	0.02	0.52		
NPQB	1.30	1.68	1.19	1.34	0.67	0.78	0.29	0.26		
Tai Po Kau	0.81	1.23	0.46	0.66	0.26	0.42	0.21	0.21		
Tsim Bei Tsui	0.20	0.94	0.39	0.92	0.34	0.75	0.14	0.26		

Table 4. Sea level acceleration (mm/yr^2) from IAP steric sea level before and after removing ENSO and PDO variabilities for a 20-year moving window.

	1993–2012		**1994–2013**		**1995–2014**		**1996–2015**		**1997–2016**	
Tide Gauge	**Before**	**After**	**Before**	**After**	**Before**	**After**	**Before**	**After**	**Before**	**After**
Dalian	−0.09	−0.10	−0.05	−0.07	−0.08	−0.11	−0.09	−0.14	0.00	−0.05
Lusi	−0.01	0.00	0.00	0.00	0.00	0.00	0.00	0.01	0.01	0.02
Kanmen	−0.10	−0.09	−0.06	−0.04	−0.06	−0.03	−0.04	0.01	0.02	0.07
Zhapo	−0.08	−0.07	0.02	0.06	−0.01	0.07	0.01	0.11	0.04	0.14
Xi Sha	−0.07	−0.05	0.16	0.23	0.25	0.45	0.32	0.72	0.20	0.68
NPQB	−0.08	−0.07	0.00	0.03	−0.03	0.04	0.00	0.09	0.02	0.11
Tai Po Kau	−0.08	−0.07	0.00	0.03	−0.03	0.04	0.00	0.09	0.02	0.11
Tsim Bei Tsui	−0.08	−0.07	0.00	0.03	−0.03	0.04	0.00	0.09	0.02	0.11
	1998–2017		1999–2018		2000–2019		2001–2020			
Tide Gauge	Before	After	Before	After	Before	After	Before	After		
Dalian	0.01	−0.03	0.03	0.00	0.01	−0.02	0.07	0.06		
Lusi	0.02	0.02	0.01	0.01	0.00	0.00	0.00	0.00		
Kanmen	0.06	0.11	0.02	0.06	0.02	0.05	0.02	0.05		
Zhapo	0.04	0.14	−0.01	0.07	−0.01	0.04	−0.05	0.00		
Xi Sha	0.18	0.50	−0.26	−0.06	−0.36	−0.13	−0.46	−0.26		
NPQB	0.03	0.11	0.00	0.07	0.01	0.06	−0.01	0.04		
Tai Po Kau	0.03	0.11	0.00	0.07	0.01	0.06	−0.01	0.04		
Tsim Bei Tsui	0.03	0.11	0.00	0.07	0.01	0.06	−0.01	0.04		

Table 5. Sea level acceleration (mm/yr^2) from tide gauge records after removing ENSO and PDO variability.

Tide Gauge	**1970–2020**	**1993–2020**
Dalian	0.03 ± 0.04	-0.12 ± 0.16
Lusi	-0.03 ± 0.04	-0.08 ± 0.18
Kanmen	0.15 ± 0.04	0.30 ± 0.20
Zhapo	0.07 ± 0.04	0.31 ± 0.20
Xi Sha	-0.30 ± 0.24 ※	0.60 ± 0.31
NPQB	0.01 ± 0.05	0.04 ± 0.20
Tai Po Kau	0.13 ± 0.05	0.20 ± 0.20
Tsim Bei Tsui	0.26 ± 0.07 ※	0.61 ± 0.23

※ Denotes tide gauge records starting later than 1970, we calculate from the record over the maximum time span between 1970–2020.

To verify the contribution of the non-steric component, we compare the sea level acceleration from the difference between satellite altimetry and IAP steric, and sea level acceleration calculated from GRACE from 2002 to 2020 (Figure 9). The spatial acceleration pattern from GRACE-based sea level data, accompanied by the difference between satellite altimetry and IAP steric sea level, show that most of the coastal locations have statistically significant positive sea level acceleration compare to the negative estimates for open ocean areas, including the Philippine Sea. However, due to the relatively short time span and coarse resolution of GRACE observations, there are some deviations from the dominant pattern. The sea level trend estimated from GRACE for 2002–2011 and 2011–2020 (Figure 10) suggests that there is an increasing contribution of mass redistribution to coastal sea level rise. It is generally consistent with the positive pattern of coastal sea level acceleration from the difference between satellite altimetry and IAP steric; thus, the increasing contribution of mass redistribution could be the main driver of coastal sea level acceleration.

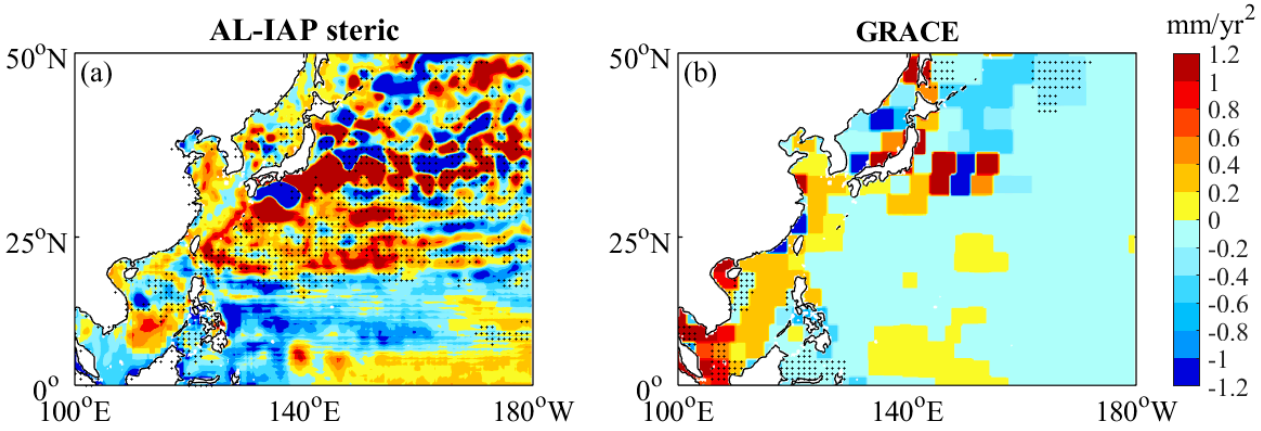

Figure 9. Sea level acceleration from the difference between satellite altimetry and IAP steric and GRACE during 2002–2020. Stippling indicates regions with no significant acceleration at the 95% level.

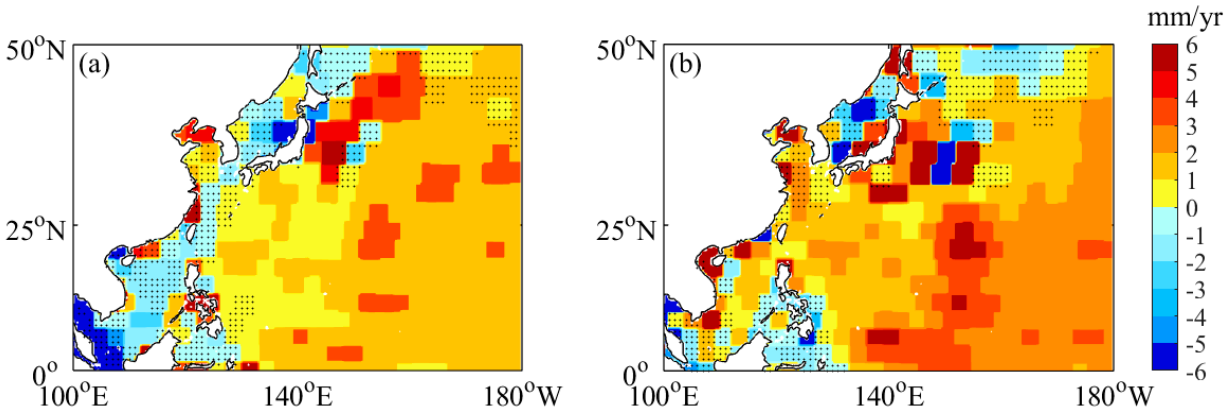

Figure 10. Sea level trend (Units: mm/yr) from GRACE for (**a**) 2002–2011 and (**b**) 2011–2020. Stippling indicates regions with no significant trend at the 95% level.

4. Discussion

4.1. The Robustness of Coastal Sea-Level-Acceleration Estimation

Individual tide gauge records show that coastal sea level accelerations range between -0.03 ± 0.04 mm/yr^2 in Lusi and 0.15 ± 0.04 mm/yr^2 in Kanmen (Table 3) after removing the ENSO and PDO variability for 1970–2020. This is consistent with estimations from Wang et al. [29] for 1970–2018, in which a recent decrease in groundwater extraction could be expected to account for the significant negative acceleration in coastal cities. There are some estimates of acceleration from previous studies [29,31], e.g., an acceleration of 0.085 ± 0.020 mm/yr^2 is detected in the Bohai Sea, while the number is 0.074 ± 0.032 mm/yr^2 in the East China Sea from the 1950s to 2013 [31]; however, there is a significant difference in time span in these studies compared with our results.

Our analysis shows that apart from Dalian, Lusi, and NPQB, other locations all show much higher accelerations than the global mean sea level estimates, after correcting for ENSO and PDO variabilities during the satellite altimetry era [14], while the neighboring station of NPQB shows a much higher acceleration than the global. A possible explanation for such a difference could be vertical land movement, which is generally assumed to be linear and not contaminating the estimate of acceleration. However, local subsidence estimates could be changed over time [32].

The reversal between positive and negative accelerations is found to be more frequent near the coastline compared with the open ocean, also suggesting that complex coastal conditions require more careful treatment to estimate the coastal sea level acceleration. However, it is difficult to determine whether coastal sea levels are accelerating from

tide gauge records as internal variability could obscure the underlying anthropogenic contribution to the acceleration calculated from short records [33–40]. For the record length of 20 years around the China coast, the range of acceleration varies greatly from -3 to 2 mm/yr^2 (Figure 1). It can be explained by the multidecadal sea-level variations that dominate the coastal sea level from 20–30 years or longer periods [41,42], and such oscillations are in part driven by natural climate variations associated with atmospheric pressure and wind stress [43,44]. The estimations of sea level acceleration calculated from tide gauge records for 1970–2020 and for 1993–2020 suggest that the uncertainty decreases hugely with the extension of record length, so it could be attributed to the removal of multidecadal variations. The scatter of sea-level-acceleration values calculated from tide gauge records around the China coast also decreases rapidly with an increase in record length; when the record length increases to more than 70 years, sea level acceleration is much smaller.

To improve the monitoring of sea level rise and acceleration, there is a need for continuous tide gauge observations [45], and an increase in tide gauge locations along the coast. The underestimation/overestimation in satellite altimetry compared with tide gauge records, which mostly results from land contamination within the radar echo [46], suggests that new altimetry sensors might improve future sea level monitoring along the coast [46].

4.2. Determining Drivers for Sea Level Acceleration over the China Seas

Our analysis suggests that steric sea level changes, associated with ENSO and PDO variabilities, are the main contributor to sea level acceleration in the Philippine Sea and its surrounding open ocean areas, supporting the previous publications [30]. Since the late 1990's, PDO has shifted to a cold phase, where the negative PDO brings cool water into this region, which reduces the positive pattern of sea level acceleration, and so, sea level acceleration from satellite altimetry and IAP steric both increase in this region with the removal of ENSO and PDO variabilities. Then, in the early 2000's, the PDO returned to a short-lived warm phase, followed by a swift return to a cold phase [30], thus the changing patterns of sea level acceleration from both satellite altimetry and IAP steric weaken during that time, as demonstrated in our study.

Along the coast, sea level acceleration could be explained by changes in the mass component, as suggested by an analysis of GRACE observations and some agreement with the difference between satellite altimetry and IAP steric sea level (Figure 9). Around the China coast, before 1997, regional sea level acceleration from satellite altimetry presented a changing pattern with the evolving of a 20-year moving window, after removing the ENSO and PDO variabilities. Sea level acceleration also changes in most tide gauge locations (Table 4), which is consistent with the changing pattern from satellite altimetry around the China coast. The changing pattern of the steric component could not account for the evolving pattern of sea level acceleration around the China coast, which reveals that steric sea level is not the main contributor to coastal sea level acceleration. The relatively short time span of the GRACE data limits our understanding of the mass contribution associated with ENSO and PDO variabilities to the evolving pattern of coastal sea level acceleration; thus, it remains unresolved whether and how the mass component is mainly contributing to the coastal sea level acceleration. Complicated coastal conditions strongly require more efforts to understand the underlying physical mechanism which drives the coastal sea level acceleration. For example, sea level acceleration calculated from tide gauge records in Dalian is consistent with steric sea level acceleration for both 1970–2020 and 1993–2020 (Table 2); however, the contribution of the steric component is not supposed to account for such acceleration in sea levels due to the shallow Bohai Sea. Instead, the ocean bottom pressure associated with external forcing, including winds and currents, is considered to play the dominant role [47]. The moving window of sea level acceleration from satellite altimetry (Table 4) and IAP steric (Table 5) also proves that the steric component is not the main contributor. The match for sea level acceleration from tide gauge records and IAP

steric sea level for certain periods is likely to be related to contamination from vertical land movement. Longer GRACE observations are necessary to study such underlying processes.

The GRACE-based sea-level-acceleration pattern reveals that the strong positive/negative accelerations in the Kuroshio and Kuroshio-extension regions [48,49] are significant. While it is insignificant based on the difference between satellite altimetry and IAP steric sea level, this could be explained by the relatively low resolution of GRACE observations, which is unable to capture all underlying processes, especially in the Kuroshio-extension region. To better interpret the physical mechanisms driving regional sea level acceleration, a higher resolution of GRACE observations is also strongly needed.

5. Conclusions

In this study, we explore the sea level acceleration around the China coast as well as over the China Seas using tide gauge records combined with high-resolution satellite altimetry. Average sea level acceleration varies from -0.05 ± 0.04 mm/yr^2 to 0.41 ± 0.32 mm/yr^2 for records ending after the 2000s. Around the China coast, sea level acceleration changes with a large variability if the record length is not long enough. To examine the evolution of acceleration for the near coastal locations and open ocean, we also calculate the moving window of sea level acceleration from satellite altimetry near the coastline and over the whole study area. It is found that sea level acceleration is more sensitive near the coastline compared with the whole study area.

The agreement between the patterns of sea level acceleration from satellite altimetry and from the steric sea level in the Philippine Sea and its surrounding deep ocean, before and after removing the ENSO and PDO variabilities, suggests that the steric sea level is the main contributor to sea level acceleration in the open ocean. The evolving acceleration pattern from satellite altimetry and IAP steric sea level after removing the ENSO and PDO variabilities, compared with before removing it, proves that the steric component mainly contributes to the evolution pattern of sea level acceleration in the Philippine Sea and its surrounding deep ocean through the PDO variations, which obscure the changing pattern of sea level acceleration. While for coastal regions, mass redistribution is considered to be the main contributor to coastal sea level acceleration in most locations, as presented by the difference between satellite altimetry and IAP steric as well as GRACE-based sea level acceleration, the physical mechanisms, however, still remain a subject for further discussion with the need for longer GRACE observations.

Author Contributions: S.J. and Y.Q. designed the study. Y.Q. and S.J. performed the analyses. Y.Q. and S.J. prepared the manuscript. Y.Q., S.J. and S.W. provided suggestions, ideas, and discussion and improved the writing of the paper. All authors have read and agreed to the published version of the manuscript.

Funding: The authors are supported by Gansu Provincial Science and Technology Program (22ZD6FA005). Y.Q. is also supported by State Key Laboratory of Earth Surface Processes and Resource Ecology (2022-ZD-05), Beijing Normal University. S.J. is supported by NERC NC International program: Future states of the global Coastal ocean: Understanding for Solutions (FOCUS: NE/X006271/1).

Data Availability Statement: The authors declare that all the sources of data supporting this study are available within the paper, and they are sufficient for the findings of this analysis.

Acknowledgments: The authors gratefully acknowledge Hindumathi Palanisamy for the helpful suggestions and Judi Wolf for general discussion and English grammar corrections.

Conflicts of Interest: The authors declare no conflict of interest.

References

1. Allan, R.P.; Hawkins, E.; Bellouin, N.; Collins, B. IPCC, 2021: Summary for Policymakers. In *Climate Change 2021: The Physical Science Basis. Contribution of Working Group I to the Sixth Assessment Report of the Intergovernmental Panel on Climate Change*; Masson-Delmotte, V., Zhai, P., Pirani, A., Connors, S.L., Péan, C., Berger, S., Caud, N., Chen, Y., Goldfarb, L., Gomis, M.I., et al., Eds.; Cambridge University Press: Cambridge, UK, 2021; pp. 3–32. [CrossRef]
2. Jevrejeva, S.; Jackson, L.P.; Grinsted, A.; Riva, R.; Moore, J.C. Coastal sea-level rise with warming above 2 degree. *Proc. Natl. Acad. Sci. USA* **2016**, *113*, 13342–13347. [CrossRef]
3. Abadie, L.M.; Jackson, L.P.; Murieta, E.S.D.; Jevrejeva, S.; Galarraga, I. Comparing urban coastal flood risk in 136 cities under two alternative sea-level projections: RCP 8.5 and an expert opinion-based high-end scenario. *Ocean Coast. Manag.* **2020**, *193*, 105249. [CrossRef]
4. Qu, Y.; Jevrejeva, S.; Williams, J.; Moore, J.C. Drivers for seasonal variability in sea level around the China seas. *Glob. Planet. Chang.* **2022**, *213*, 103819. [CrossRef]
5. Church, J.A.; White, N.J. A 20th century acceleration in global sea-level rise. *Geophys. Res. Lett.* **2006**, *33*, L01602. [CrossRef]
6. Haigh, I.D.; Wahl, T.; Rohling, E.J.; Price, R.M.; Pattiaratchi, C.B.; Calafat, F.M.; Dangendorf, S. Timescales for detecting a significant acceleration in sea-level rise. *Nat. Commun.* **2014**, *5*, 3635. [CrossRef] [PubMed]
7. Kemp, A.C.; Horton, B.P.; Donnelly, J.P.; Mann, M.E.; Vermeer, M.; Rahmstorf, S. Climate related sea-level variations over the past two millennia. *Proc. Natl. Acad. Sci. USA* **2011**, *108*, 11017–11022. [CrossRef] [PubMed]
8. Jevrejeva, S.; Moore, J.C.; Grinsted, A.; Woodworth, P.L. Recent global sea-level acceleration started 200 years ago? *Geophys. Res. Lett.* **2008**, *35*, L08715. [CrossRef]
9. Woodworth, P.L.; White, N.J.; Jevrejeva, S.; Holgate, S.J.; Church, J.A.; Gehrels, W.R. Evidence for the accelerations of sea level on multi- decade and century timescales. *Int. J. Climatol.* **2009**, *29*, 777–789. [CrossRef]
10. Feng, X.; Tsimplis, M.N. Sea level extremes at the coasts of China. *J. Geophys. Res. Ocean.* **2014**, *119*, 1593–1608. [CrossRef]
11. He, Q.; Bertness, M.D.; Bruno, J.F.; Li, B.; Chen, G.; Coverdale, T.C.; Altieri, A.H.; Bai, J.; Sun, T.; Pennings, S.C.; et al. Economic development and coastal ecosystem change in China. *Sci. Rep.* **2014**, *4*, 5995. [CrossRef]
12. Chen, C.; Zuo, J.; Chen, M.; Gao, Z.-G.; Shum, C.-K. Sea level change under IPCC-A2 scenario in Bohai, Yellow and East China Seas. *Water Sci. Eng.* **2014**, *7*, 446–456.
13. Qu, Y.; Jevrejeva, S.; Jackson, L.P.; Moore, J.C. Coastal sea level rise around the China Seas. *Glob. Planet. Chang.* **2018**, *172*, 454–463. [CrossRef]
14. Nerem, R.S.; Beckley, B.D.; Fasullo, J.T.; Hamlington, B.D.; Masters, D.; Mitchum, G.T. Climate-change-driven accelerated sea-level rise detected in the altimeter era. *Proc. Natl. Acad. Sci. USA* **2018**, *115*, 2022–2025. [CrossRef] [PubMed]
15. Hamlington, B.D.; Frederikse, T.; Nerem, R.S.; Fasullo, J.T.; Adhikari, S. Investigating the acceleration of re gional sea level rise during the satellite altimeter era. *Geophys. Res. Lett.* **2020**, *47*, e2019GL086528. [CrossRef]
16. Moreira, L.; Cazenave, A.; Palanisamy, H. Influence of interannual variability in estimating the rate and acceleration of present-day global mean sea level. *Glob. Planet. Chang.* **2021**, *199*, 103450. [CrossRef]
17. Holgate, S.J.; Matthews, A.; Woodworth, P.L.; Rickards, L.; Tamisiea, M.E.; Bradshaw, E.; Foden, P.R.; Gordon, K.M.; Jevrejeva, S.; Pugh, J.P. New Data Systems and Products at the Permanent Service for Mean Sea Level. *J. Coast. Res.* **2013**, *29*, 493–504. [CrossRef]
18. Permanent Service for Mean Sea Level (PSMSL). Tide Gauge Data. 2022. Available online: http://www.psmsl.org/data/obtaining/ (accessed on 21 March 2022).
19. Ding, X.; Zheng, D.; Chen, Y.; Chao, J.; Li, Z. Sea level change in Hong Kong from tide gauge measurements of 1954–1999. *J. Geod.* **2001**, *74*, 683–689. [CrossRef]
20. Kalnay, E.; Kanamitsu, M.; Kistler, R.; Collins, W.; Deaven, D.; Gandin, L.; Iredell, M.; Saha, S.; White, G.; Woollen, J.; et al. The NCEP/NCAR 40-year reanalysis project. *Bull. Am. Meteorol. Soc.* **1996**, *77*, 437e470. [CrossRef]
21. Cheng, L.; Trenberth, K.E.; Fasullo, J.; Boyer, T.; Abraham, J.; Zhu, J. Improved estimates of ocean heat content from 1960 to 2015. *Sci. Adv.* **2017**, *3*, e1601545. [CrossRef]
22. Cheng, L.; Zhu, J.; Cowley, R.; Boyer, T.; Wijffels, S. Time, Probe Type, and Temperature Variable Bias Corrections to Historical Expendable Bathythermograph Observations. *J. Atmos. Ocean. Technol.* **2014**, *31*, 8. [CrossRef]
23. Tapley, D.B.; Bettadpur, S.; Ries, J.C. GRACE measurements of mass variability in the Earth system. *Science* **2004**, *305*, 503–505. [CrossRef]
24. Chambers, D.P. Observing seasonal steric sea level variations with GRACE and altimetry. *J. Geophys. Res.* **2006**, *111*, C03010. [CrossRef]
25. Cheng, X.; Li, L.; Du, Y.; Wang, J.; Huang, R.-X. Mass-induced sea level change in the northwestern North Pacific and its contribution to total sea level change. *Geo. Res. Lett.* **2013**, *40*, 3975–3980. [CrossRef]
26. Royston, S.; Watson, C.S.; Legresy, B.; King, M.A.; Church, J.A.; Bos, M.S. Sea-level trend uncertainty with Pacific climatic variability and temporally-correlated noise. *J. Geophys. Res. Ocean.* **2018**, *123*, 1978–1993. [CrossRef]
27. Zhang, L.; Delworth, T.L. Analysis of the characteristics and mechanisms of the Pacific decadal oscillation in a suite of coupled models from the Geophysical Fluid Dynamics Laboratory. *J. Clim.* **2015**, *28*, 7678–7701. [CrossRef]
28. Veng, T.; Andersen, O.B. Consolidating sea level acceleration estimates from satellite altimetry. *Adv. Space Res.* **2020**, *68*, 496–503. [CrossRef]

29. Wang, J.; Church, J.A.; Zhang, X.; Chen, X. Reconciling global mean and regional sea level change in projections and observations. *Nat. Commun.* **2021**, *12*, 990. [CrossRef] [PubMed]
30. Zhang, X.; Church, J.A. Sea level trends, interannual and decadal variability in the Pacific Ocean. *Geophys. Res. Lett.* **2012**, *39*, L21701. [CrossRef]
31. Cheng, Y.C.; Ezer, T.; Hamlington, B.D. Sea Level Acceleration in the China Seas. *Water* **2016**, *8*, 293. [CrossRef]
32. Wöppelmann, G.; Marcos, M. Vertical land motion as a key to understanding sea level change and variability. *Rev. Geophys.* **2016**, *54*, 64–92. [CrossRef]
33. Calafat, F.M.; Chambers, D.P. Quantifying recent acceleration in sea-level unrelated to internal climate variability. *Geophys. Res. Lett.* **2013**, *40*, 3661–3666. [CrossRef]
34. Chen, X.; Zhang, X.; Church, J.A.; Watson, C.S.; King, M.A.; Monselesan, D.; Legresy, B.; Harig, C. The increasing rate of global mean sea-level rise during 1993–2014. *Nat. Clim. Chang.* **2017**, *7*, 492–495. [CrossRef]
35. Dangendorf, S.; Rybski, D.; Mudersbach, C.; Müller, A.; Kaufmann, E.; Zorita, E.; Jensen, J. Evidence for long-term memory in sea-level. *Geophys. Res. Lett.* **2014**, *41*, 5530–5537. [CrossRef]
36. Han, W.; Meehl, G.A.; Stammer, D.; Hu, A.; Hamlington, B.; Kenigson, J.; Palanisamy, H.; Thompson, P. Spatial patterns of sea-level variability associated with natural internal climate modes. *Surv. Geophys.* **2017**, *38*, 217–250. [CrossRef] [PubMed]
37. Wenzel, M.; Schröter, J. Reconstruction of regional mean sea level anomalies from 595 tide gauges using neural networks. *J. Geophys. Res. Atmos.* **2010**, *115*, C08013. [CrossRef]
38. Douglas, B.C. Global sea level acceleration. *J. Geophys. Res.* **1992**, *97*, 12699–12706. [CrossRef]
39. Woodworth, P.L. A search for accelerations in records of European mean sea level. *Int. J. Clin Matology* **1990**, *10*, 129–143. [CrossRef]
40. Houston, J.R. Sea-Level Acceleration: Analysis of the World's High-Quality Tide Gauges. *J. Coast. Res.* **2021**, *37*, 272–279. [CrossRef]
41. Jevrejeva, S.; Grinsted, A.; Moore, J.C.; Holgate, S. Nonlinear trends and multiyear cycles in sea level records. *J. Geophys. Res.* **2006**, *111*, C09012. [CrossRef]
42. Holgate, S.J. On the decadal rates of sea level change during the twentieth century. *Geophys. Res. Lett.* **2007**, *34*, L01602. [CrossRef]
43. Bromirski, P.D.; Miller, A.J.; Flick, R.E.; Auad, G. Dynamical suppression of sea level rise along the Pacific Coast of North America: Indications for imminent acceleration. *J. Geophys. Res. Ocean.* **2011**, *116*, C7. [CrossRef]
44. Sturges, W.; Douglas, B.C. Wind effects on estimates of sea level rise. *J. Geophys. Res. Ocean.* **2011**, *116*, C06008. [CrossRef]
45. Iz, H.B.; Shum, C.K. Minimum record length for detecting a prospective uniform sea level acceleration at a tide gauge station. *All. Earth* **2022**, *34*, 8–15. [CrossRef]
46. The Climate Change Initiative Coastal Sea Level Team. Coastal sea level anomalies and associated trends from Jason satellite altimetry over 2002–2018. *Sci. Data* **2020**, *7*, 357. [CrossRef]
47. Liu, H.; Cheng, X.; Qin, J.; Zhou, G.; Jiang, L. The dynamic mechanism of sea level variations in the Bohai Sea and Yellow Sea. *Clim. Dyn.* **2023**, *61*, 1–11. [CrossRef]
48. Sakamoto, T.T.; Hasumi, H.; Ishii, M.; Emori, S.; Suzuki, T.; Nishimura, T.; Sumi, A. Responses of the Kuroshio and the Kuroshio Extension to global warming in a high-resolution climate model. *Geophys. Res. Lett.* **2005**, 32. [CrossRef]
49. Cheng, X.; Zhao, M.; Duan, W.; Jiang, L.; Chen, J.; Yang, C.; Zhou, Y. Regime shift of the sea level trend in the South China Sea modulated by the tropical Pacific decadal variability. *Geophys. Res. Lett.* **2023**, *50*, e2022GL102708. [CrossRef]

Disclaimer/Publisher's Note: The statements, opinions and data contained in all publications are solely those of the individual author(s) and contributor(s) and not of MDPI and/or the editor(s). MDPI and/or the editor(s) disclaim responsibility for any injury to people or property resulting from any ideas, methods, instructions or products referred to in the content.